Journal of Alloys and Compounds xxx (xxxx) 170808

Contents lists available at ScienceDirect

Journal of Alloys and Compounds

journal homepage: www.elsevier.com/locate/jallcom

Electrodeposited rhenium sandwich structures with thermal expansion mismatch and the superconducting transition behaviors

Kamal Ahammed [a], Seyed Morteza Taghavi Kouzehkanan [b], Tae-Sik Oh [b], Qiang Huang [a]

[a] Department of Chemical and Biological Engineering, University of Alabama, Tuscaloosa, AL 35487, USA
[b] Department of Chemical Engineering, Auburn University, Auburn, AL 36849, USA

ARTICLE INFO

Article history:
Received 5 April 2023
Received in revised form 27 May 2023
Accepted 30 May 2023

ABSTRACT

The effects of stress and strain on the superconducting transition behavior of electrodeposited Re film are investigated using sandwich structures, where a thin Re layer is deposited in between thicker metal layers with different coefficients of thermal expansion (CTE), such as Cr and Cu. The entire sandwich structures are prepared using electrodeposition at room temperature. Cyclic voltammetry is conducted to characterize the electrochemical behavior of metal deposition. X-ray fluorescence, scanning electron microscope, X-ray diffraction, electrical resistance measurements at cryogenic temperature, and in-situ X-ray diffraction are utilized to characterize the electrodeposited films in the stacks. The Re films sandwiched between metals with different CTEs show different superconducting transition and recrystallization behaviors. This study provides an innovative method to inhibit grain growth and to maintain an enhanced critical temperature of the electrodeposited amorphous superconducting Re.

1. Introduction

Superconducting materials are becoming increasingly important for electronic applications such as quantum computers, which aim to solve a range of challenging problems currently unachievable with conventional computing technology. The operation of cryogenic quantum computers relies on qubits implemented with superconducting Josephson junctions cooled down to 10 mK by a dilution refrigerator [1]. Thermal noises due to Joule heating significantly reduce the performance of such computers. Other additional classical electronic components are operated at higher temperatures in connection with the qubits using coaxial lines [1]. These interconnects typically run through different temperature stages of the dilution refrigerator. A stage temperature above 4 K can be easily achieved using liquid helium with a boiling point of 4.2 K. Superconducting materials with an elevated superconducting transition temperature or critical temperature (T_c) above 4.2 K are suitable for interconnects at or below this temperature stage. Such interconnects eliminate the concern of joule heating.

Although Superconducting materials such as Niobium (Nb) and its alloys (Nb-N, Nb-Ti, and Nb-Ti-N) with T_c up to 9.2 K [2] are widely used in superconducting magnets [3], adverse effects on superconducting behavior due to oxidation in circuitry limit their applications [4,5]. Applications of other superconducting candidates like Lead (Pb) with T_c 7.2 K [6] and their alloys are limited because of environmental concerns [7]. On the contrary, having one of the highest melting points among all elements [8], substantial mechanical strength, hardness, high electrical impedance [9], and good diffusion barrier properties [10–13], Re and its alloys stand out to be promising alternatives not only in superconducting computers but also in the production of special coatings [14].

Electrodeposition is considered as a cost-effective, controllable, scalable, and facile process for material deposition [15]. It has been extensively used in circuit fabrication [16–18]. Electrodeposition of bright, hard deposits of amorphous Re and its alloys from aqueous solution has been reported with enhanced current efficiency [19–24]. While the bulk crystalline Re is a type-I superconductor with a T_c of about 1.7 K [25,26], an elevated T_c up to 6 K has been reported in electroplated amorphous Re [27]. In addition to controlling the crystallinity of the film, the effects of altering the crystal lattice have also been studied. For example, an enhanced T_c of about 3 K has been reported for bulk Re under shear strain using high-pressure torsion [28]. Re doped with foreign elements such as Tungsten (W) and Osmium (Os) have also been shown to increase the T_c [29]. In addition, an increase in T_c to about 2.65 K is observed for Re doped with interstitial Carbon (C) atom, where the crystalline lattice expands upon doping [30]. While these studies have shown the effects of stress or lattice strain on the superconductivity, some other effects are typically convoluted. While the high-pressure torsion method introduces shear strain on the metal, it also refines grain size and creates high density defectivities, both of which also have profound impacts on the superconductivity [31]. On the other

E-mail address: qhuang@eng.ua.edu (Q. Huang).

https://doi.org/10.1016/j.jallcom.2023.170808
0925-8388/

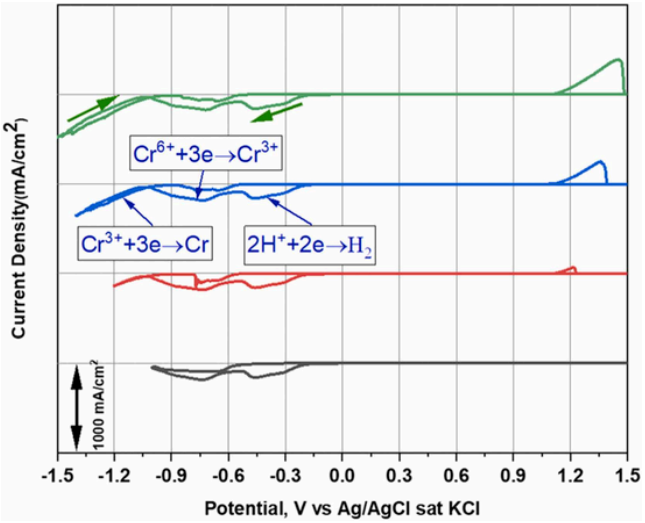

Fig. 1. CV Studies for Cr deposition on Pt for different potential ranges in electrolyte containing 1 M CrO_3 and 0.01 M H_2SO_4 solution at a scan rate of 20 mV/s and a solution agitation of 400 RPM.

hand, the chemical doping method inevitably introduces chemical effects in addition to altering the lattice size.

This paper attempts to study the effects of strain or stress on superconductivity using an alternative way, taking advantage of the different thermal expansion behaviors of materials. To our best knowledge, studies using such an approach have not been reported yet. In this effort, we electrodeposit sandwich structures with Re in between other metals with different CTEs to introduce compressive or tensile stresses on Re as the temperature decreases. A systematic study is conducted using these sandwich structures on the effects of CTE mismatch on the superconducting transition and recrystallization behaviors of the Re layer.

2. Experimental

A three-compartment electrochemical cell with a glass frit to separate the analyte and catholyte is used in this study. A silver chloride (Ag/AgCl) electrode with saturated potassium chloride, connected to the catholyte with a capillary, is used as the reference electrode. All cyclic voltammetry (CV) studies are conducted against this reference electrode. The outer surface of the reference electrode is washed with deionized water and air-blown dried before each experiment to avoid solution contamination and addition of excessive water. A platinum rotating disk electrode (RDE) with a surface area of 0.196 cm^2 is used for CV studies. Silicon coupons with gold patterns, comprising a 10 mm long and 1 mm wide strip connected to a 3 mm by 5 mm contact pad, are used as the substrates to deposit Re films, Cu-Re-Cu, and Cr-Re-Cr sandwich structures. The fabrication of such pattern substrates are detailed elsewhere [32]. A holder that rotates similarly to an RDE is used to mount the Si coupon. Electrical connection from the holder to the substrate is made through a spring-loaded U-shaped metal pin landing on the Au contact pad. The external surface of the pin, except for the end tip, is coated with Teflon to ensure good insulation.

Three electrolytes adapted from literatures are used in this study. The Re electrolyte contains 0.025 M NH_4ReO_4, 0.1 M H_2SO_4, and 5 M LiCl [19,32]. The Cu electrolyte contains 0.63 M $CuSO_4$, 0.1 M H_2SO_4, 1.4 mM HCl, and 300 ppm polyethylene glycol (PEG) [33–35]. The Cr electrolyte contains 1 M CrO_3 and 0.01 M H_2SO_4, corresponding to a CrO_3 to H_2SO_4 ratio of 100:1 [36,37].

Three steps are involved in the fabrication of Cu-Re-Cu sandwich sample. In the first step, a Cu layer is deposited on the Au substrate at a constant current density of − 5 mA/cm^2 using the Cu solution. Then, the Re layer is deposited on the Cu layer at a constant voltage of − 1 V from the Re solution. Finally, another Cu layer is deposited on the Re layer using the same condition as the first Cu layer. The Cr-Re-Cr sandwich sample is deposited using the similar approach. The Cr layers are deposited using a constant current of − 430 mA/cm^2 and the Re layer is still deposited at a constant voltage of −1 V. Non-sandwiched Re films alone are also deposited on the Au substrate for comparison. The deposition time for Re, Cu, and Cr layers in sandwich structures are fixed at 600 s, 600, and 120 s, respectively. The rotation rate for all deposition is fixed at 400 RPM. A Cu foil (99.9%) is used as the anode for Cu deposition, and a Pt foil (99.99%) is used for Re and Cr. An Autolab 302 N potentiostat is used for all the deposition and other electrochemical studies. All samples in this study are fabricated at room temperature. All chemicals used in this study are at least ACS grade, and deionized water with a resistivity of 18 MΩ-cm is used in all experiments.

A Bruker X-ray fluorescence (XRF) spectrometer operating at 50 kV, and 800 μA is used to determine the sample thickness (only during process development). An FEI Quanta 200 3D Focused Ion Beam (FIB) station is used to cross-section the samples. A ThermoFisher Apreo Field Emission Scanning Electron Microscope (FE-SEM) is used to observe the cross-section. A home-built vacuum annealing chamber operated at a pressure below 1×10^{-4} Torr is used to anneal the samples at elevated temperatures. Crystallographic analysis is carried out using a Bruker D8 power X-ray diffractometer with Cobalt (Co) K_α source (wavelength = 1.79 Å). Another Anton Paar theta-2theta diffractometer with Cu K_α source (wavelength = 1.54 Å), where the ambient and temperature are precisely controlled, is used to analyze the recrystallization behavior of Re during annealing. The temperature is ramped at a rate of 1 ºC/min, and a 10-second diffractogram snapshot is taken for every 10 ºC. A Quantum Design Dynacool Physical Property Measurement System (PPMS) is utilized to measure the film resistance and determine the superconducting critical temperature (T_c). A constant direct current (DC) of 1 mA is applied for the measurement. Each sample is electrically bridged to the resistivity puck through aluminum wires using DuPont 4929 N™ silver conductor paste. The resistance is measured with PPMS with a 4-probe configuration with temperature scanned from 30 K down to 1.8 K. An adiabatic demagnetization refrigerator (ADR) attachment is used to enable the measurement down to a temperature of about 0.1 K.

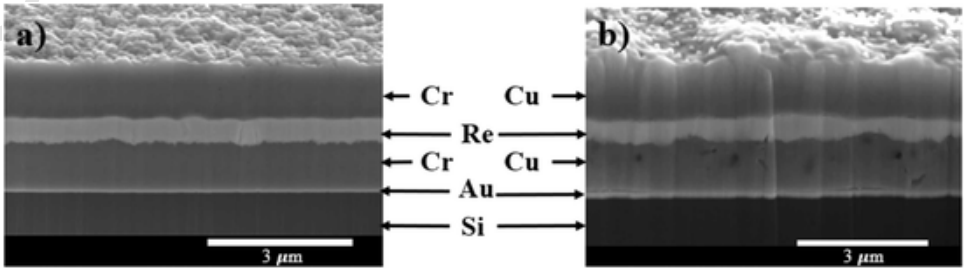

Fig. 2. Cross-section images of a) Cr-Re-Cr b) Cu-Re-Cu sandwich structures.

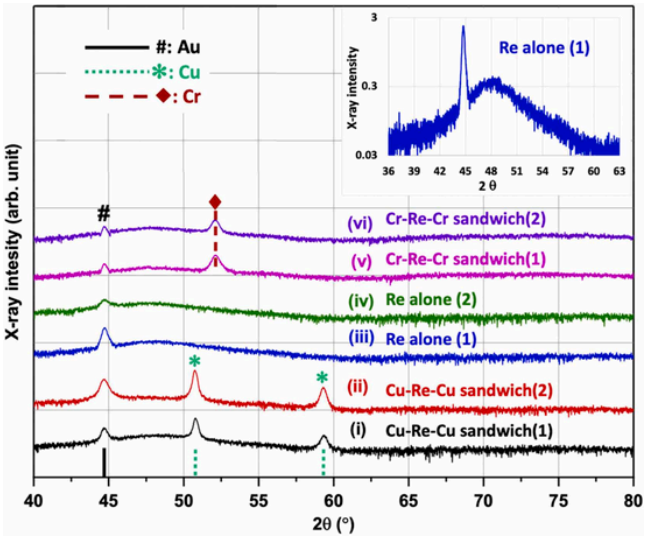

Fig. 3. XRD patterns for as deposited Re in different structures, with one example pattern from the standalone Re film in the inset.

3. Results and discussions

Electrochemical Study – The electrodeposition behaviors of Cu and Re in the same electrolytes used here have been well studied. CV studies are only carried out to understand the electrochemical behavior of Cr on Pt in this report. Fig. 1 shows the results of Cr deposition for different potential ranges in the Cr electrolyte at a rotation rate of 400 RPM. Anodic current, i.e., Cr stripping, observed as a peak starting at 1.1 V is used as an indicator for the presence of Cr metal. In other words, the presence of this anodic peak shows the deposition of Cr in the previous cathodic condition and the integrated area of this anodic peak shows the amount of Cr deposited on Pt. Fig. 1 clear shows that the Cr deposition occurs only when the cathodic potential reaches – 1.2 V or below. And further decreasing the cathodic potential results in more Cr to be deposited and a larger peak area in the anodic stripping. In all cases, the first cathodic current during the forward scan, between – 0.4 and – 0.5 V, is due to proton reduction, shown in Fig. 1. Afterward, multiple cathodic current steps are observed for Cr electrodeposition during the negative scan in conjunction with the stripping peak in anodic scan, indicating metallic Cr is formed through multiple-step reduction processes, i.e., step 1: $Cr^{6+} + 3e \rightarrow Cr^{3+}$; *step* 2: $Cr^{3+} + 3e \rightarrow$ Cr, consistent with previous literature [38]. Although solution agitation is present during the CV study, a decline in cathodic current is observed for step 1, i.e., $Cr^{6+} + 3e \rightarrow Cr^{3+}$. Two factors may contribute to this behavior. Firstly, passivation of the surface by films containing chromium ions. The formation of Cr^{3+} in the presence of sulphate ions will lead to a soluble species. However, if the production rate of this Cr^{3+} ion exceeds the sulfate supply, the formation of chromic dichromate or chromic chromate will take place on the reaction surface. The latter presumably act as insoluble mixed oxide films, causing a decline in cathodic current density. Secondly, oxide or hydroxide films are also likely to form at potentials where hydrogen evolution dominates, leading to an increased pH at the Pt electrode surface [38] and decreasing the current density. A constant current density of – 430 mA/cm^2 will be used to deposit Cr layers for the fabrication of Cr-Re-Cr sandwich structures. As Fig. 1 shows, this current density approximately corresponds to cathodic potential of – 1.5 V in the CV. The second step of Cr reduction reaction (instead of hydrogen evolution) dominate, and metallic Cr is formed at this condition.

Structural Characterization of Sandwich – Fig. 2(a) and (b) show the SEM images of a FIB prepared section within the sandwich samples. A clear adherent interface between Re and Cu or between Re and Cr without any apparent delamination is observed for both stack samples, confirming the successful formation of the sandwich structure using the electrodeposition method. The thickness of the layers are about 500 nm for Re, 1 μm for both Cu and Cr. Not only are the Re layer of same thickness between the two different sandwich structures, the deposition processes of Cu and Cr are also adjusted to achieve approximately same thickness for better comparison. Small voids are observed, but only in one of the Cu layers, probably due to an artifact from FIB cross sectioning. One small difference between the two sandwich structures is that the bottom Cu layer has a higher roughness than Cr layer, resulting in a slightly higher variation in Re layer thickness.

Fig. 3 shows the XRD patterns of the sandwich structures as well as the single Re layer electrodeposited on Au seed. Two duplicated samples are fabricated for each of the three types of structure (Re in sandwich or by itself). The Re layer thickness is controlled between 500–600 nm and the capping layer thickness is approximately twice as the Re layers. The thickness is measured using XRF but also calibrated and confirmed using SEM. The y-axis in Fig. 3 and all other XRD Figures in this report, i.e., the X-ray intensity of the samples, is plotted in log scale to ease the comparison. The only strong sharp peaks observed across all samples are from Au seed, Cr, or Cu layers. A broad background peak at 2θ between 40º to 57º is observed for all samples. A FWHM of 5.6º can be determined from the inset for the reflection at 2θ of 48º for Re film alone, corresponding to an average grain size of 2.5 nm. This nanocrystalline nature with similar grain size is observed for all the as deposit films in Fig. 1 regardless of the sandwich configu-

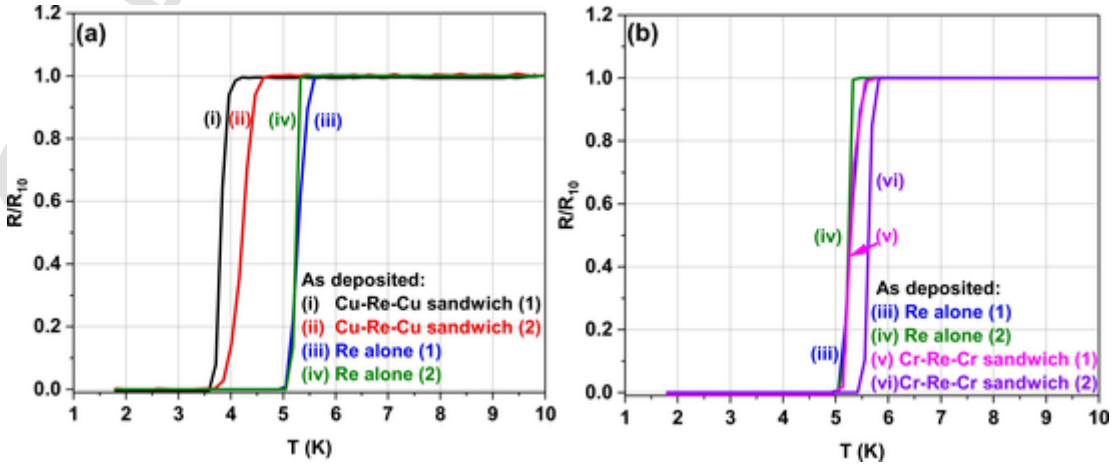

Fig. 4. Film resistance normalized with resistance at 10 K along with temperature sweep for Re in different structures.

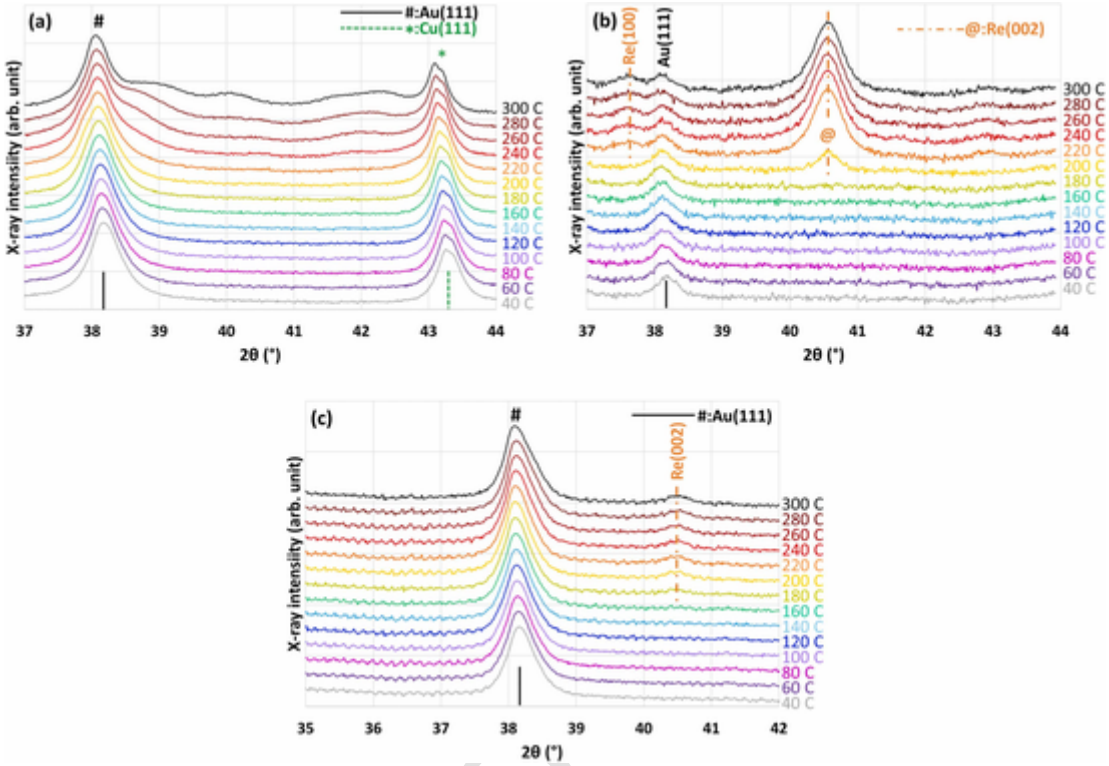

Fig. 5. In situ XRD patterns along with temperature ramping at a rate of 10 °C/min for (a) Cu-Re-Cu, (b) free Re, and (c) Cr-Re-Cr samples.

ration and is consistent with previous studies for Re films alone [32, 39].

Superconductivity – Fig. 4 shows the superconducting transition of the same samples characterized by XRD in Fig. 3. The resistance is normalized with the resistance at 10 K. It is known that the T_c of electrodeposited Re film may vary between 4 and 6 K as the thickness changes between 90 and 850 nm [39]. However, all the Re layers are deposited using identical conditions in this study, where the process reproducibility is demonstrated with the SEM characterization in Fig. 2.

Yet, two duplicates are included in this study to minimize such uncertainty. It is evident from Fig. 4 that all samples show sharp transition to the superconducting state and the behaviors of the duplicated samples are almost identical, further demonstrating the good reproducibility of the deposition processes. As depicted in Fig. 4(a), the T_c of electrodeposited amorphous Re film alone is 5.2 K, consistent with previous studies. However, when being sandwiched between Cu layers, the T_c of Re decreases to 3.6 – 4.2 K. On the other hand, this transition for Re films between Cr layers occurs at 5.2 – 5.5 K, approximately unchanged from the un-sandwiched Re alone, as shown in Fig. 4(b).

Cu, Re, and Cr have the CTE of 16.5×10^{-6} K^{-1}, 6.2×10^{-6} K^{-1}, and 4.9×10^{-6} K^{-1}, [40], respectively. Having significantly higher CTE than the Re, Cu contracts more than the Re when the temperature decreases. Assuming the as-deposit layers are strain free or of negligible strain at room temperature, Cu is expected to induce a compressive strain on Re in Cu-Re-Cu structure during resistance measurement at a cryogenic temperature. On the contrary, having a slightly lower CTE than Re, Cr contracts similarly or slightly less than Re upon cooling. Therefore, the Re layer between Cr layers experiences no stress or very weak tensile stress upon the temperature decrease. It worth mentioning that the CTE of amorphous Re is not available. However, it is not uncommon for amorphous and crystalline metals to have similar CTEs [41–43]. Furthermore, these CTEs are based on room temperature measurements and may vary along with temperature. In addition, the Young's modulus and other mechanical properties also depend on temperature and crystallinity. Therefore, it is believed that the CTEs listed above provides a relative comparison between the three metals and enables a qualitative discussion.

Chu et al. [44] reported that the T_c decreases upon application of pressure for both single and polycrystalline Re samples. In addition, Masaki et al. [28] tuned the T_c of Re by applying shear strain on polycrystalline Re, where the T_c increases upon the expansion of unit cell. Furthermore, Zhu et al. [30] elevated the T_c of crystalline Re by alloying it with interstitial C atoms, which causes anisotropic lattice expansion on the hexagonal Re structure. The observations in this study appear to be consistent with these reports with other effects such as induced defectivities and foreign doping elements excluded.

Recrystallization and superconductivity – The temperature at which the as deposit amorphous Re recrystallizes is determined using in situ XRD measurements along with temperature ramping in N_2 ambient. The XRD snapshots from room temperature up to 300 ºC for a Cu-Re-Cu sandwich, a Re single layer, and a Cr-Re-Cr sandwich are shown in Fig. 5. It is worth mentioning that each sample used in this set of experiment is made using the same condition as the other samples of similar type used for XRD and superconductivity measurements. A narrow 2θ range is selected to include Re(100), Re(002), and Re(101) reflections at 37.59°, 40.45°, and 42.89° at room temperature, respectively. It is also worth noting here that as the x-ray sources are different between the in-situ XRD and static XRD measurements and the peak positions are also different between these measurements. In addition, the in-situ XRD setup may have small instrument offset in 2θ, which has been corrected using the standard Au(111) peak position. Due to the thermal expansion of metals, a drift toward slightly lower 2θ position can be observed along temperature increase and the Au(111) peak at 30 °C is used for this correction. As shown in Fig. 5(b) for the case of Re films alone, the Re(100) and Re(002) peaks appear at a temperature of 220 and 200 ºC, respectively, consistent with previous studies [39]. For Cu-Re-Cu sample, no peak corresponding to Re is observed for the temperature sweep up to 300 °C, shown in Fig. 5(a). In addition, several broad peaks between 38.5° and 43° appears at elevated tempera-

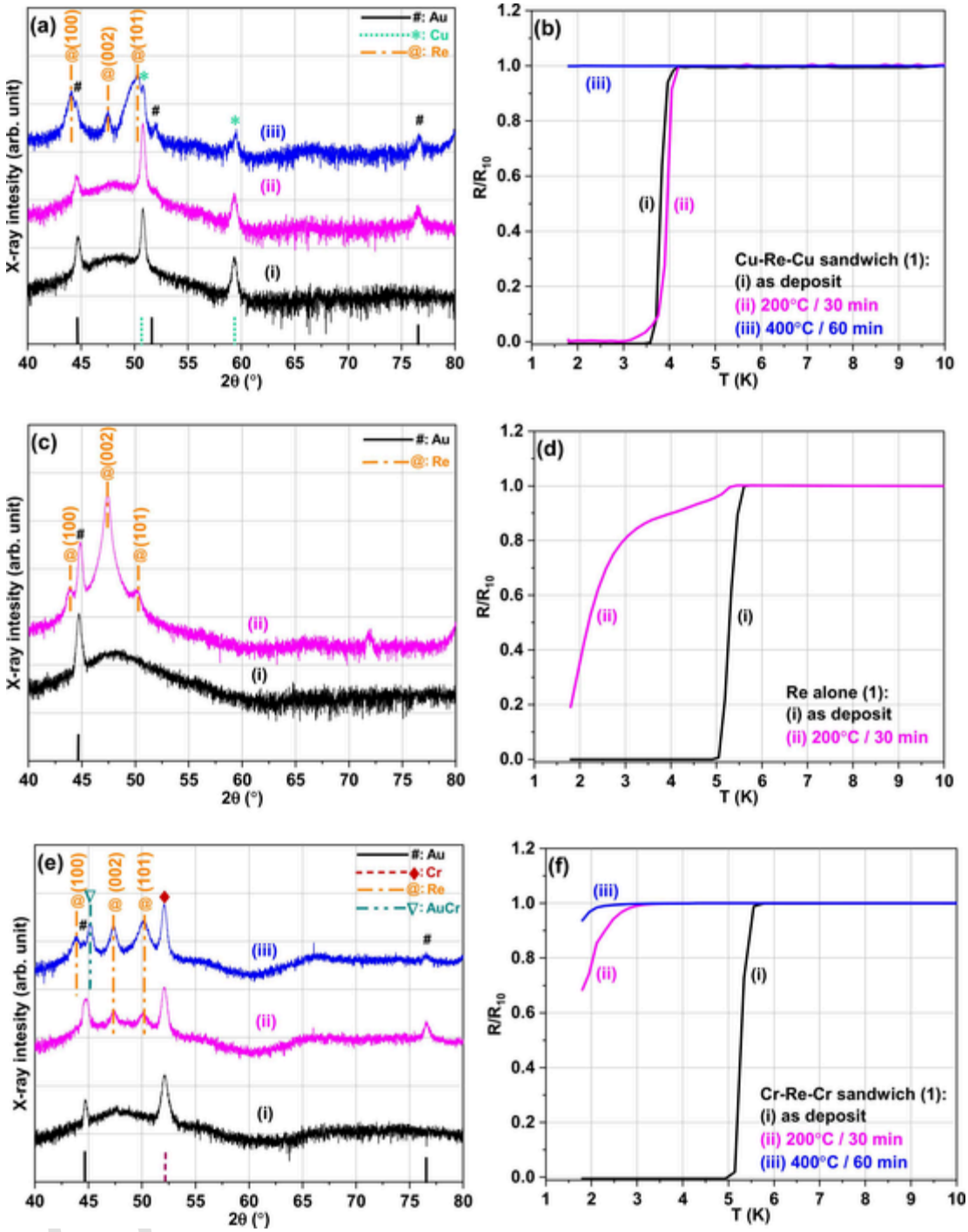

Fig. 6. (a, c, e) XRD patterns and (b, d, f) film resistance normalized with resistance at 10 K along with temperature sweep for as deposited and thermally annealed (a-b) Cu-Re-Cu, (c-d) Re alone, and (e-f) Cr-Re-Cr sample.

tures above 280 °C, indicating possible intermixing and formation of nanocrystalline intermetallic phase between Au and Cu [45]. On the other hand, as shown in Fig. 5(c), the Re(002) peak for Cr-Re-Cr sandwich structure becomes visible at a slightly lower temperature of 180 ºC. In addition, at an even higher temperature of 380 ºC (not shown in the plot), a peak with a slightly higher 2θ position than Au(111) peak has emerged, indictive of the formation of a solid solution with Cr in Au and a decreased size of Au lattice [46].

Recrystallization of amorphous or nanocrystalline materials, or grain coarsening, involves grain boundary annihilation and atom rearrangement, resulting in an overall volume shrinkage [47]. As mentioned in the preceding sections, the thermal expansion behavior of Re, Cu, and Cr are different during temperature ramping. During annealing at an elevated temperature, a single Re layer expands without any restrictions resulting in recrystallization at a temperature of 200 ºC, consistent with recrystallization of a free Re layer of similar thickness reported in previous literature [39]. However, having a higher CTE than Re, Cu tends to expand more than the Re, inducing tensile stress on the Re layer in the Cu-Re-Cu sandwich. Such tensile stress appears to hinder the volume shrinkage or recrystallization of Re in between Cu. As a result, no Re peak is observed for Re films in such stacks. On the other hand, Cr, which has a slightly lower CTE than Re, expands slightly less

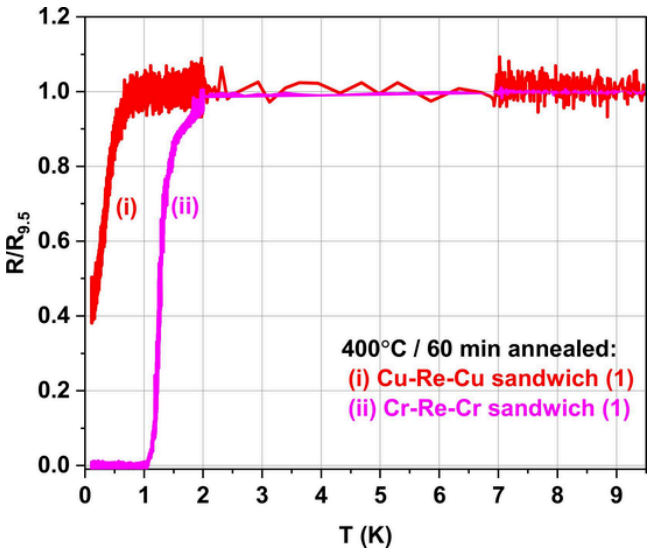

Fig. 7. Film resistance normalized with resistance at 9.5 K along with temperature sweep for thermally annealed Re in sandwich structures.

than Re or similar to Re when the temperature is elevated, inducing a weak compressive stress on the Re layer in between Cr. This appears to have marginally facilitated the volume shrinkage of Re in Cr-Re-Cr sample and the Re peak emerges at a slightly lower temperature of about 180 °C.

To establish a link between the superconductivity and the recrystallization of Re on various structures, additional tests are conducted on the same samples used for XRD and superconductivity measurements in Figs. 3 and 4, respectively. These tests involve annealing the samples at different temperatures for a specific duration and characterizing them using XRD and PPMS techniques.

Fig. 6 shows the results of these tests. The Re(002) peak emerges in free Re and Cr-Re-Cr samples after annealing at 200 ºC for 30 min. The Cu-Re-Cu sandwich does not show any Re peak at this condition, suggesting that the 200 ºC for 30 min annealing is insufficient to crystallize Re, which is also consistent with in-situ XRD results. At the same time, the T_c of Re is suppressed for free Re and Cr-Re-Cr due to the recrystallization, whilst the Re layer in Cu-Re-Cu maintains a similar T_c as the as deposit structure. This clearly demonstrates an innovative way to inhibit the recrystallization and maintain the enhanced Tc of electrodeposited amorphous Re despite of thermal processing.

Further annealing of the sandwich samples at 400 ºC for 60 min leads to the recrystallization of Re in both samples. No peaks corresponding to any intermetallic compound of Re with Cu or Cr are observed at this annealing condition, consistent with the literatures [46, 48]. However, peak shifting for Au(111) or emergence of a new peak has also been observed toward a slightly higher 2θ value due to the formation of solid solution of Cr in Au at this high temperature [46], decreasing the lattice size of elemental Au. This is also observed in the in-situ XRD results. This solid solution formation may also occur between Au and the bottom Cu layer in Cu-Re-Cu sandwich. But the XRD results in Fig. 6(a) seems to suggest a much less degree for this reaction and the Au and Cu peaks are still discernable with little shift. Resistance measurements for these 400 °C annealed sandwich samples show little to no superconducting transition above 1.8 K, consistent with the recrystallization of Re in both structures.

An ADR attachment is used in conjunction with the PPMS in a further attempt to determine the T_c of these sandwich samples annealed at 400 ºC for 60 min. The results are presented in Fig. 7. The data acquisition is much less frequent between 7 and 2 K, resulting in less noisy curves. The metal layers in stack structures are expected to be fully relaxed after annealing at this high temperature of 400 ºC [49]. During the T_c measurement, the Re layer in Cu-Re-Cu structure experiences high compressive stress due to the significant difference in thermal expansion between Cu and Re causing lower T_c from the Re bulk value of 1.7 K. On the contrary, having a slightly lower CTE than Re, Cr induces a weak to no tensile stress in Re in Cr-Re-Cr stack which results in T_c similar to the intrinsic T_c of Re in crystalline form.

4. Conclusion

Sandwich structures comprising layers with thermal expansion mismatch are successfully electrodeposited to study the effects of stress and strain on the superconducting transition and recrystallization of amorphous Re without introducing other chemical and mechanical effects. Re films sandwiched between Cu, which have a higher coefficient of thermal expansion (CTE) than Re, show a suppressed T_c. This decrease in T_c is due to the compressive stress generated on the Re films at cryogenic temperature. Conversely, when Re films are in between Cr with a similar or slightly lower CTE than the Re, the T_c remains almost unchanged from a single stand-alone Re layer. While the effects of tensile stress is expected to be opposite to compressive stress, the extremely weak tensile stress generated in the Re films while cooling the Cr-Re-Cr sample in PPMS is insufficient to significantly increase the T_c of the Re films. On the other hand, the stresses on the Re films in Cu-Re-Cu and Cr-Re-Cr stacks become opposite during thermal annealing at elevated temperatures, i.e., tensile for Cu-Re-Cu and compressive for Cr-Re-Cr. The recrystallization of electrodeposited amorphous Re during this thermal annealing is inhibited in the former case, whilst it is slightly facilitated in the latter. As the enhanced T_c observed for amorphous Re typically degrades upon grain coarsening, the Cu-Re-Cu sandwich structure withstands 200 °C annealing showing no degradation in T_c. On the other hand, the Cr-Re-Cr sandwich as well as the Re film alone do not reach superconducting state above 1.8 K after the same annealing. This finding provides new direction to inhibit or to control grain growth during thermal annealing and to improve the reliability of amorphous superconductors with enhanced critical temperature.

CRediT authorship contribution statement

Kamal Ahammed : Data curation, Investigation, Formal analysis, Writing – original draft. **Seyed Morteza Taghavi Kouzehkanan :** Data curation, Investigation. **Tae-Sik Oh :** Investigation, Formal analysis. **Qiang Huang :** Conceptualization, Formal analysis, Writing – original draft, Writing – review & editing.

Declaration of Competing Interest

The authors declare the following financial interests/personal relationships which may be considered as potential competing interests: Qiang Huang reports financial support was provided by National Science Foundation.

Data Availability

Data will be made available on request.

Acknowledgements

National Science Foundation is acknowledged for support through grants 1941820 and 2016541. The Alabama Analytical Research Center, College of Engineering Analytical Facility, and A&S glass shop at the University of Alabama are acknowledged for characterization and for making the parts used in this study. Dr. Tom Hogan at Quantum Design is acknowledged for the ADR measurements. Dr. Mark Weaver and Dr. Sushma Kotru are acknowledged for a helpful discussion on the mechanical property of nanocrystalline metals.

References

[1] S. Krinner, et al., Engineering cryogenic setups for 100-qubit scale superconducting circuit systems, EPJ Quantum Technol. 6 (1) (2019) 2.
[2] D. Patel, et al., Niobium-titanium (Nb-Ti) superconducting joints for persistent-mode operation, Sci. Rep. 9 (1) (2019).
[3] C. Laverick, Niobium demand and superconductor applications: an overview, J. Less Common Met. 139 (1) (1988) 107–122.
[4] J. Halbritter, On the oxidation and on the superconductivity of niobium, Appl. Phys. A 43 (1) (1987) 1–28.
[5] T.F. Harrelson, et al., Elucidating the local atomic and electronic structure of amorphous oxidized superconducting niobium films, Appl. Phys. Lett. 119 (24) (2021) 244004.
[6] J. Eisenstein, Superconducting elements, Rev. Mod. Phys. 26 (3) (1954) 277–291.
[7] M. Arra, et al., Study of immersion silver and tin printed-circuit-board surface finishes in lead-free solder applications, J. Electron. Mater. 33 (9) (2004) 977–990.
[8] I.L. Shabalin, Rhenium, Springer, Netherlands, 2014, pp. 317–357.
[9] E. Salakhova,2014. The Electrochemical Deposition of Rhenium Chalcogenides from Different Electrolytes. 2014. 1: p. 185–198.
[10] R. Ghasemi, Z. Valefi, Electrodeposition of rhenium-base layer as a diffusion barrier between the NiCoCrAlY coating and a Ni-based superalloy, J. Alloy. Compd. 732 (2018) 470–485.
[11] F. Lang, T. Narita, Improvement in oxidation resistance of a Ni3Al-based superalloy IC6 by rhenium-based diffusion barrier coatings, Intermetallics 15 (4) (2007) 599–606.
[12] T. Narita, et al., Application of rhenium coating as a diffusion barrier to improve the high temperature oxidation resistance of nickel based superalloy, Corrosion (2001) 2001. p. NACE-01157.
[13] Y. Wang, S. Ohnuki, T. Narita, Formation process of a rhenium-based diffusion barrier on a nickel-based superalloy, MRS Proc. 980 (2006).
[14] Adelmann, C., et al. Alternative metals for advanced interconnects. IEEE.
[15] M.J. Aus, et al., Electrical, magnetic and mechanical properties of nanocrystalline nickel, MRS Online Proc. Libr. 318 (1) (1993) 39–44.
[16] H. Deligianni, S. Ahmed, L.T. Romankiw, The next frontier: electrodeposition for solar cell fabrication, Interface Mag. 20 (2) (2011) 47–53.
[17] T.P. Moffat, D. Josell, Superconformal Electrodeposition for 3-Dimensional Interconnects, Isr. J. Chem. 50 (3) (2010) 312–320.
[18] Nakano, H., et al. Advanced trench filling process by selective copper electrodeposition for ultra fine printed wiring board fabrication. IEEE.
[19] Q. Huang, T.W. Lyons, Electrodeposition of rhenium with suppressed hydrogen evolution from water-in-salt electrolyte, Electrochem. Commun. 93 (2018) 53–56.
[20] A. Naor, N. Eliaz, E. Gileadi, Electrodeposition of rhenium–nickel alloys from aqueous solutions, Electrochim. Acta 54 (25) (2009) 6028–6035.
[21] A. Naor-Pomerantz, N. Eliaz, E. Gileadi, Electrodeposition of rhenium–tin nanowires, Electrochim. Acta 56 (18) (2011) 6361–6370.
[22] L.E. Netherton, M.L. Holt, Electrodeposition of rhenium from aqueous solutions, J. Electrochem. Soc. 95 (6) (1949) 324.
[23] V.V. Zhulikov, Y.D. Gamburg, Electrodeposition of rhenium and its alloys, Russ. J. Electrochem. 52 (9) (2016) 847–857.
[24] C.G. Fink, P. Deren, Rhenium plating, Trans. Electrochem. Soc. 66 (1) (1934) 471.
[25] J.K. Hulm, Superconductivity of pure metallic rhenium, Phys. Rev. 94 (5) (1954) 1390–1391.
[26] J.K. Hulm, B.B. Goodman, Superconducting properties of rhenium, ruthenium, and osmium, Phys. Rev. 106 (4) (1957) 659–671.
[27] D.P. Pappas, et al., Enhanced superconducting transition temperature in electroplated rhenium, Appl. Phys. Lett. 112 (18) (2018) 182601.
[28] M. Mito, et al., Large enhancement of superconducting transition temperature in single-element superconducting rhenium by shear strain, Sci. Rep. 6 (1) (2016) 36337.
[29] C.W. Chu, W.L. McMillan, H.L. Luo, Superconductivity of Re-Os, Re-Ru, Ru-Os, and Re-W hcp alloy systems and slightly doped Re, Phys. Rev. B 3 (11) (1971) 3757–3762.
[30] Q. Zhu, et al., Anisotropic lattice expansion and enhancement of superconductivity induced by interstitial carbon doping in Rhenium, J. Alloy. Compd. 878 (2021) 160290.
[31] R. Idczak, et al., Influence of severe plastic deformation on superconducting properties of Re and, Phys. C: Supercond. Appl. 590 (2021) 1353945.
[32] Q. Huang, Y. Hu, Electrodeposition of superconducting rhenium with water-in-salt electrolyte, J. Electrochem. Soc. 165 (16) (2018) D796–D801.
[33] Q. Huang, et al., Leveler effect and oscillatory behavior during copper electroplating, J. Electrochem. Soc. 159 (9) (2012) D526–D531.
[34] J.J. Kelly, C. Tian, A.C. West, Leveling and microstructural effects of additives for copper electrodeposition, J. Electrochem. Soc. 146 (7) (1999) 2540–2545.
[35] M. Hasegawa, et al., Effects of additives on copper electrodeposition in submicrometer trenches, J. Electrochem. Soc. 152 (4) (2005) C221.
[36] A. Brenner, P. Burkhead, C.T. Jennings, Physical properties of electrodeposited chromium, J. Res. Natl. Bur. Stand. 40 (1948) 31.
[37] W. Hume-Rothery, M.R.J. Wyllie, The structure of electro-deposited chromium, Proc. R. Soc. Lond. Ser. A. Math. Phys. Sci. 181 (987) (1943) 331–344.
[38] J. Lin-Cai, D. Pletcher, The electrochemical study of a chromium plating bath. I. Reactions leading to solution-free species, J. Appl. Electrochem. 13 (2) (1983) 235–243.
[39] W.D. Sides, et al., Grain growth and superconductivity of rhenium electrodeposited from water-in-salt electrolytes, J. Appl. Phys. 127 (8) (2020) 085301.
[40] W.M. Haynes, D.R. Lide, T.J. Bruno, CRC handbook of chemistry and physics, CRC Press, 2016.
[41] J.E. Shelby, Thermal expansion of amorphous metals, J. Non-Cryst. Solids 34 (1) (1979) 111–119.
[42] R. Birringer, Nanocrystalline materials, Mater. Sci. Eng.: A 117 (1989) 33–43.
[43] M.M. de Lima Jr, et al., Coefficient of thermal expansion and elastic modulus of thin films, J. Appl. Phys. 86 (9) (1999) 4936–4942.
[44] C.W. Chu, T.F. Smith, W.E. Gardner, Study of fermi-surface topology changes in rhenium and dilute Re solid solutions fromTcMeasurements at high pressure, Phys. Rev. B 1 (1) (1970) 214–221.
[45] P. Villars, L.D. Calvert, W.B. Pearson, Pearson's handbook of crystallographic data for intermetallic phases, Am. Soc. Met. 1985 (1985) 3258 Vol. 1, 2, 3.
[46] T.B. Massalski, et al., Binary alloy phase diagrams, Am. Soc. Met. (1986).
[47] L. Benedetti, et al., Shrinkage behaviour of semi-crystalline polymers in laser sintering: PEKK and PA12, Mater. Des. 181 (2019) 107906.
[48] Du, Y., M Materials Science International Team, Cu-Re Binary Phase Diagram Evaluation·Phase diagrams, crystallographic and thermodynamic data: Datasheet from MSI Eureka in SpringerMaterials ⟨(https://materials.springer.com/msi/docs/sm_msi_r_20_013904_01)⟩. MSI Materials Science International Services GmbH.
[49] D.H. Herring, Stress relief, Wire Form. Technol. Int. 13 (3) (2010) 26–28.